Chapter 5

Investigating Recent Changes in Observed Surface Humidity and Possible Causes

SUMMARY

The gridded land and marine data are combined to create a near global product HadCRUH in specific and relative humidity. This is used to assess recent changes in humidity at a range of spatial scales and compared to the global temperature record and for comparison with GCMs.

Humidity and temperature have a complex and non-linear relationship. In a water unlimited environment, in accordance with the Clausius-Clapeyron relation (section 1.2), the magnitude of potential change in specific humidity depends strongly on both ambient temperature and changes in temperature. Relative humidity is generally assumed to be conserved over long time periods such that specific humidity is expected to increase exponentially with temperature. It has already been noted (Chapters 3 and 4) that on average the Globe is moistening significantly (in absolute terms). Changes in relative humidity are of mixed sign although mostly negative, and significant at a range of scales in the marine data. There is, however, a likely spurious positive bias in the pre-1982 marine data that if non-climatic in origin may result in overestimation of negative trends. A direct comparison of these changes with recent changes in temperature enables an assessment of how closely HadCRUH adheres to the Clausius-Clapeyron relation. Furthermore, the temperature and humidity records used here are produced independently from each other. These analyses therefore go some way to assessing the validity of both HadCRUH and the global temperature record as reliable representations of global climate. To this end HadCRUH is analysed alongside the global surface temperature data set HadCRUT3 (Brohan *et al.*, 2006).

GCMs are becoming ever more important to enhancing our understanding of the global climate system (section 1.6). While model output includes both specific humidity and relative humidity, to date very little model assessment uses these fields beyond testing for a near-constant relative humidity. This is largely due to the lack of a high-quality observational humidity dataset with which to compare. Hence, a comparison of HadCRUH timeseries and trends with GCM output provides valuable insights including simple validation of modelled humidity and some very basic detection and attribution of climatic change aspects.

5.1 BLENDING THE LAND AND MARINE GRIDDED DATA

The land and marine components of HadCRUH are combined following the methods of Jones *et al.* (2001) without variance corrections for sampling density. For grid-boxes containing both components, each value is weighted according to the proportional spatial presence of land in that grid-box. However, neither component is allowed to be weighted less than 25 %. This method originates from small oceanic island *T* data likely being more reliable than surrounding *SST* data (Jones *et al.*, 2001). Whether this is the case for humidity or not, such a convention is desirable because it allows representation of both components within one grid-box. This method assumes that the two components, although created using slightly different techniques, are sufficiently similar.

To investigate this assumption, timeseries and trends in *q* from both components for the Globe, Hemispheres and Tropics (Chapter 3 (land) and 4 (marine)) are compared (Table 5.1). The presence of strong, spatially coherent and significant trends in *q* makes it a better candidate than *RH* for such a comparison. Trends are of a similar sign, magnitude and significance. They are larger for land data except for the Southern Hemisphere. Land and marine timeseries correlate well with high (~0.7) *r* values in all but the Southern Hemisphere where problems of data coverage and quality have already been noted. Correlations for post-1982 (marine shift – section 4.4) are very slightly stronger in all regions except for the Tropics – the marine shift is not so obviously apparent in this region in the marine *q* series.

5.2 HUMIDITY AND TEMPERATURE - HADCRUH AND HADCRUT3

HadCRUT3 is the latest version of a long standing and well studied surface *T* dataset (Brohan *et al.*, 2006). The marine component is based on the *SST* data set HadSST2 (Rayner *et al.*, 2006) which originates largely from the same sources as marine HadCRUH, and structural methods for creating the marine gridded data are near identical (Chapter 4). The land component differs from HadCRUH in source dataset, although many observing stations are in both. Methods for quality control and homogenisation also differ. HadCRUT3 monthly mean anomalies for 1973 to 2003 at a 5 ^{o} by 5 ^{o} grid-box resolution are extracted and re-normalised to the 1974 to 2003 climatology period of HadCRUH such that the mean over that period is zero. The more globally complete HadCRUT3 dataset has been sub-sampled to HadCRUH field availability.

5.2.1 How do Changes in T, q and RH Compare on a Global and Hemispheric Scale?

In all regionally averaged timeseries (Globe, Hemispheres and Tropics – Fig. 5.1) low temporal resolution variability in *q* and *T* is very similar in sign and relative magnitude. This is as might be expected following Clausius-Clapeyron theory under the assumption of constant *RH*. Indeed, high (>0.7) *r* values are obtained from *q*-*T* correlations (at the monthly mean anomaly resolution) in all regions except the Southern Hemisphere. These are largest in the Tropics and seasonally in Northern Hemisphere JJA and SON (not shown). *RH* is much more independent. Timeseries of *T* and *q* are slightly offset pre-1982 (anomalies are more negative in *T*) coinciding with the marine shift (section 4.4), and begin to diverge from 1998 (anomalies more positive in *T*). The *RH* record shows consistent positive anomalies pre-1982 and a decrease towards the end of the record (where *T* and *q* divergence is largest), in the Tropics and Southern Hemisphere but not in the Northern Hemisphere. The 1998 divergence is most apparent in the Northern Hemisphere. Although there is no reason why the *q* record should follow *T* so closely in water limited environments, the close agreement of *T* and *q* between 1982 and 1998 and precise timing of these disparities (correlating with suspected marine data issues) offers further support to the hypothesis that the trend in marine *q* is underestimated (section 4.4). These effects, if they are really non-climatic artefacts, have the effect of reducing global (blended land and marine) estimates of changes in *q* in HadCRUH.

For regional averages over the Globe, Northern Hemisphere and Tropics, trends are positive and highly significant (at the 1 % level) in both *T* and *q* (Table 5.2). The assumption of constant *RH* (section 1.2) appears robust over most but not all regions and scales as trends are generally not significant except for the Tropics, Northern Hemisphere MAM, JJA and SON and Southern Hemisphere JJA. All *RH* trends are negative apart from in the Northern Hemisphere. The Clausius-Clapeyron relation states that under constant *RH* the water holding capacity of the air will rise exponentially. These findings from HadCRUH, on these large spatial scales and long time scales, demonstrate that where the ability of the atmosphere to hold more water vapour increases, so too does the actual water vapour content. HadCRUH trends in *q* are strongest in the Tropics and the Northern Hemisphere Summer season, which, as regions/seasons of relatively higher ambient *T* and available water is also consistent with the Clausius-Clapeyron relation. This assessment is important both for validating HadCRUH within the realms of theoretical physics and also resolving a well known theory over large spatial and temporal scales.

With a global mean *T* of ~14 ^{o}C (Jones *et al.*, 1999), a change of 0.18 ^{o}C 10yr^{-1} (Global *T* trend from HadCRUT3) could be expected to bring about a change in *q* (assuming *RH* is 70 %) of ~0.08 g kg^{-1} 10yr^{-1}. The Global *q* trend is only very slightly less than this (0.07 g kg^{-1} 10yr^{-1}) (likely underestimated due to the marine 1982 shift). Along with the high *r* values and Clausius-Clapeyron relation concurrence (on large scales) discussed above, this gives weight to HadCRUH as a reasonable source of global humidity data over the period and provides a degree of independent corroboration for HadCRUT3.

5.2.2 How do Changes in T, q and RH Compare on a Regional Scale?

From grid-box analyses of land and marine *q* and *RH* (section 3.4.2 and 4.3.2 respectively) it is clear that humidity exhibits regional changes worthy of further investigation. Twenty nine regions are chosen following their use by Giorgi & Francisco (2000) and in the IPCC (Giorgi *et al.*, 2001) and timeseries and trends analysed (Fig. 5.2 (locations and abbreviations) and Figs. 5.3a and b). Most regions are mainly over land with marine regions which are large in size, so although widely used, there is little climatic significance to this choice of regions.

Trends in T and q are positive in all regions except where q trends are indistinguishable from zero (Central America, North Australia and South Australia). For *RH*, 12 regions exhibit significant (at 1 % and 5 % levels) trends of either sign (eight negative and four positive). This supports previous findings that while over large spatial scales the assumption of constant *RH* is supported, this is not the case at the smaller regional scale where strong variations exist.

Four regions show both significant (at 1 % and 5 % levels) actual and relative moistening trends: eastern North America; North Asia; South Asia; and the Tibetan Plateau. In this context 'actual' refers to increasing water content of the atmosphere denoted by increases in q as opposed to relative moistening (closeness to saturation) inferred by *RH*. This is explained and justified in section 2.3. No regions show significant actual and relative drying. The strongest significant moistening occurs jointly over the Tibetan Plateau and the North Atlantic for q and the Tibetan Plateau for *RH* whereas the strongest drying for *RH* occurs in the Amazon. Other regions of interest are listed in Table 5.3.

Correlations of T-q and T-*RH* timeseries are produced for all regions. All T-q correlations are positive with only six regions giving r less than 0.6 (Tibetan Plateau, North Australia, South Pacific, Central America, Sahara and South Africa). For *RH* there are no r values greater than 0.5 or less than -0.4. As with the previous larger scale analysis, these findings corroborate the humidity record from HadCRUH following the Clausius-Clapeyron relation of increasing humidity with temperature and further substantiate the Global T record HadCRUT3.

To investigate further the expectation that the water content of the air will rise as the water holding capacity increases (under increasing T), observed absolute (as opposed to anomaly) q is compared with estimated absolute q derived from observed absolute T at a constant *RH* of 70 % and 100 % using equations described in Chapter 2. This is calculated seasonally for each region. For each region, the observed and estimated q timeseries are plotted along with observed absolute *RH* (Fig. 5.4 for five example regions). In general, observed absolute q lies within a reasonable range of that prescribed by observed changes in absolute *T* and observed absolute *RH*, further verifying the scientific value of HadCRUH. Alaska and North West Canada, North Asia (not shown) and the Tibetan Plateau are the exceptions as in DJF and SON the observed absolute *q* exceeds that prescribed even by 100 % RH. However, this is most likely due to increased inaccuracy of humidity conversion algorithms at very low humidity and temperature which is exacerbated by converting away from the source resolution (seasonally as opposed to hourly) (McCarthy & Willett, 2006).

Trends are calculated for estimated and observed *q* for each season (also shown in Fig. 5.4). Of these, 53 % of trends are below and 19% within the range of trends given by estimated *q* at 70 % and 100 % *RH*. A further 14 % of trends are negative when estimated trends are positive. The above is to be expected considering that water availability is usually a limiting factor. In total, the vast majority (86 %) of observed trends show good agreement with the concept of rising water content with rising water holding capacity as expressed by the Clausius-Clapeyron relation. A further 14 % are above the range of estimated trends. The Tibetan Plateau (Fig. 5.4) has larger observed trends in all seasons. This suggests that increases in humidity on regional scales are not solely dependent on *T* although data quality here may be an issue. It should be noted that these findings are very preliminary and further investigation is required.

5.2.3 How do Changes in T, q and RH Compare at the Grid-box Scale?

Correlating *T* and *q* monthly mean and seasonal anomaly timeseries for each grid-box gives consistently strong and positive correlations in the Northern Hemisphere and Tropical Pacific. These are positive for almost the entire Globe and stronger at the seasonal time scale (Figure 5.5). These findings support HadCRUH as a relatively reliable record of surface humidity.

5.2.4 Implications of the Combined Humidity and Temperature Analysis

The above findings simultaneously corroborate both HadCRUH and HadCRUT3 as realistic climate records. As such, HadCRUH can be of significant use to the climate community. For *T* the regions of highest signal-to-noise ratio, and therefore regions of high potential for climate change detection and attribution studies, were found to be in the mid-latitudes of the Northern Hemisphere, especially in the Summer season (Wigley & Jones, 1981). Likewise for q, the Northern Hemisphere Summer signal is strong, however, in addition the Tropics exhibit strong signals. This may make q a favourable diagnostic for detection and attribution.

In terms of the moist enthalpy component of the energy budget (section 1.1) the energy needed to warm a parcel of air increases non-linearly with increasing moisture. Thus the overall picture of warming and moistening in the Northern Hemisphere and Globally points towards more positive trends in near-surface energy in the climate system than implied by temperature changes alone, and is of interest for further study. In hurricane prone regions this may be of interest especially following the record North Atlantic hurricane activity of 2005 (Trenberth & Shea, 2006; Anthes *et al*., 2006; Santer *et al*., 2006).

The substantiation of HadCRUH alongside HadCRUT3 at a range of spatial scales bodes well for future potential of a heat stress product incorporating humidity. The historical record of humidity from HadCRUH provides previously unavailable insight into spatial and temporal changes of humidity essential for ascertaining trends in heat stress and accurately forecasting future impacts.

5.3 SPECIFIC HUMIDITY IN HADCM3 – INVESTIGATING POSSIBLE CAUSES

GCMs have become increasingly useful tools over the last decade to investigate causes of observed climate changes and project future possible climates for different scenarios. The primary diagnostic has traditionally been T and GCMs can now do a reasonable job at representing recently observed changes (Stott *et al.*, 2000; Stott *et al*., 2006). Humidity is a relatively unstudied variable when it comes to models. Thus HadCRUH provides the opportunity to investigate the representation of humidity in a GCM in addition to possible causes of recent changes.

There are many GCMs (section 1.6) available today. The latest Hadley Centre GCM, HadGEM1, is desirable to use as it includes land use change as a forcing which is likely important to surface humidity, and better represents direct and indirect effects of aerosols than its predecessor HadCM3 (Stott *et al*., 2006). However, for the purpose of this study, HadCM3 (Gordon *et al.*, 2000; Pope *et al.*, 2000) is used for a number of reasons. It is a well studied ocean-atmosphere coupled model. Its representation of ENSO events, which are strong in HadCRUH timeseries, is superior to that of HadGEM1 (Johns *et al*., 2006; Stott *et al*., 2006). More crucially, there are more runs containing humidity output available for HadCM3.

Due to the limited previous work undertaken with HadCM3 humidity (and modelled humidity generally), model output is first necessarily extracted from the Hadley Centre archive which is time consuming. Multiple runs suitable for ensemble creation are only available for Control, Natural only and Anthropogenic only forcings (see Tett *et al*., 2002 for a discussion of forcing details). The Natural ensemble is forced by volcanic output and solar irradiance. The Anthropogenic ensemble is forced by greenhouse gases, ozone and sulphate emissions (Stott *et al*., 2000). Output in q is only available at daily 3.75 ^{o} by 2.5 ^{o} grid-box resolution and so it is re-gridded by bilinear interpolation to 5 ^{o} by 5 ^{o} grid-box monthly mean anomalies for subsequent masking to match HadCRUH spatial and temporal coverage. In total, four runs comprise each ensemble mean henceforth referred to as NATURAL and ANTHRO. Both ensembles end in 1999. To account for this, the climatological period is modified to 1974 to 1999 and HadCRUH re-normalised to that period. All trends are calculated over the period 1973 to 1999 for consistency between timeseries. In the absence of the availability of an all forcings ensemble, as an approximation, the ANTHRO and NATURAL ensembles are summed to give an all forcings ensemble. This is referred to as ANT+NAT. For the Control run, 31 year timeseries are extracted at overlapping 10 year intervals from a total length of 301 years resulting in 27 control timeseries in total. These are normalised to years 2-27 for each resulting timeseries, consistent with the other ensembles. Following the approach of Stott *et al*. (2006) the range of trends from these control runs is used to give a measure of natural variability within the climate system at a range of scales.

Prior to any analysis between observed and modelled humidity it is useful to check how well the model reconstructs the basics of the climate system in terms of the climatology. This is done by comparing the climatology from the observations to the HadCM3 climatology which is the mean climatology from the 27 control run segments. The climatology period is from 1974 to 1999 (2 to 27 for the control segments) in keeping with that of the ANTHRO and NATURAL ensembles. Figure 5.6 shows the CONTROL climatology and observations minus CONTROL climatology for January and July. The zonal structure of q seen in the observations is clear in the CONTROL climatology and the range is very similar although slightly larger (0 to ~23 g kg^{-1}). The HadCM3 climatology both under- and overestimates q relative to the observations with poorer agreement over the Northern Hemisphere Summer months (June to August). However, for the most part differences are within ± 1 g kg^{-1} and the general structure is represented such that HadCM3 is considered suitable for comparison with HadCRUH.

5.3.1 Comparing HadCM3 and HadCRUH at Large Spatial Scales

Similar to Stott *et al*. (2006), regionally averaged q timeseries and trends (for the Globe, Hemispheres and Tropics – described in Table 5.1) are compared to those from the ANTHRO, NATURAL and ANT+NAT ensembles and CONTROL segments (Fig. 5.7). Any region where the observed trend exceeds the range (5^{th} to 95^{th} percentiles) given by the CONTROL segments can be considered significant as this implies that the observed trend is very unlikely to be solely due to natural internal variability. This is the case in the Northern Hemisphere only, further supporting previous discussion of a potentially high signal-to-noise ratio in this region.

The ANTHRO and ANT+NAT trends are positive and significant, consistently exceeding both the CONTROL segment trend range of natural variability and the observations. They are closest to the observed trends in the Northern Hemisphere and the ANTHRO ensemble is closest to the observed trends of all the ensembles. It should be remembered that the observed trend is likely slightly underestimated due to the 1982 marine shift (section 4.4) and thus may actually be closer to the ANTHRO and ANT+NAT runs than shown here. The NATURAL ensemble hugely underestimates the observed trends. These findings point to a likely anthropogenic origin of the observed trends on large spatial scales, and a detectable anthropogenic climate change signal in q in the Northern Hemisphere.

5.3.2 Comparing HadCM3 and HadCRUH at Regional Scales

The 29 regions discussed in section 5.2.2 are used here for analysis at regional scales (Figs. 5.8 and 5.9). There are 11 regions where observed trends are greater than the measure of natural internal variability given by the CONTROL segments and thus can be said to exhibit a strong climate change signal. However, the majority of regions are within this measure suggesting the climate change signal is less detectable at smaller scales in concurrence with findings of Stott & Tett (1998) in their study of observed and modelled *T*. In general, the ANTHRO and ANT+NAT ensembles are better representations of the observed trends than NATURAL supporting arguments for anthropogenic origin, at least in part, of observed changes in *q*. This implies that NATURAL has very little power in explaining the long-term change component in the observations. However, at this scale it is not possible to say that one of ANTHRO or ANT+NAT performs better than the other.

5.3.3 Comparing HadCM3 and HadCRUH at the Grid-box Scale

Finally, observed grid-box *q* trends are compared to the range of natural internal variability provided by the CONTROL segments (Fig. 5.10). This is for the purpose of identifying regions with a strong climate change signal at the grid-box scale. Three further comparisons are undertaken using observation minus model (ANTHRO, NATURAL and ANT+NAT) grid-box trends for *q* following the approach of Stott *et al.* (2000) (Fig. 5.10). These are for the purpose of assessing the validity of modelled humidity on a grid-box scale and to decipher the most likely cause - natural forcings, anthropogenic forcings, or both.

In terms of climate signal detection, 33 % of the observed area exhibits trends greater than that which can be expected due to natural variability. These are mostly positive trends and clustered in the Northern Hemisphere especially in the low latitude Atlantic and Asia. In terms of attribution, Stott *et al*. (2000), who also used HadCM3, found both natural and anthropogenic forcings to have contributed significantly to 20th century *T* changes. The all forcings ensemble best represented the observations. However, they found that the natural only forcings ensemble was more critical in explaining early 20th Century changes, and the anthropogenic only forcings ensemble the latter 20th Century changes. This is consistent with a growing anthropogenic forcing footprint on the climate system.

Regarding humidity, the NATURAL ensemble trends over 1973-1999 are mostly very close to zero. Consequently, the 'observations minus NATURAL' trend pattern is almost spatially identical to that of the straight comparison of the observed trends to the measure of natural variability given by the CONTROL segments. The residual trends are mainly of significant moistening thus undermining the argument for an entirely NATURAL origin to recently observed changes. The ANTHRO ensemble best represents observed *q* trends such that 74 % of the observed grid-box trends are statistically indistinguishable from ANTHRO grid-box trends. Regions where ANTHRO and observed trends differ significantly are more patchy and of mixed sign further pointing to anthropogenic origin of observed *q* trends. Following Stott *et al.*'s findings it might be expected that an anthropogenic and natural combined forcings run (all forcings) should perform best. However, the ANT+NAT ensemble used here performs slightly worse than the ANTHRO (72 % of observed minus ANT+NAT trends are within natural variability). This may well be due to the method used to construct ANT+NAT where a linear summation may not be appropriate. Spatial coverage of trend differences is very similar to that of ANTHRO. There are also similarities with the Stott *et al.* *T* panels for an all forcings ensemble minus the observations, where trends are overestimated in the south west Pacific and underestimated in western Canada.

5.4 CONCLUSIONS

A blended humidity product HadCRUH has been created for *q* and *RH* and compared with the global *T* record from HadCRUT3 and model output *q* from HadCM3 at a range of spatial scales. Key findings are summarised below:

- Timeseries and trends in *q* and *T* correlate strongly on all scales. The observations show consistency with Clausius-Clapeyron theory at all spatial scales where as the water holding capacity of the atmosphere increases, surface water content also increases. This is not the case for all small scale regions however.
- *RH* remains near constant at all scales but trends are significant for some regions suggesting that the assumption of near-constant *RH* is not always robust.

- The two data sources of q and T have been developed separately, and over land are entirely independent in terms of structural processes. Thus the strong correlation between the two corroborates both HadCRUH and HadCRUT3 as grossly adequate climate records.
- Trends in q are largest in the Tropics and Northern Hemisphere Summer and a climate change signal in q above the noise of natural variability is detectable in the Northern Hemisphere implying that q may be a favourable diagnostic for formal detection and attribution studies.
- All comparisons with the GCM HadCM3 at a range of scales point to anthropogenic origin at least in part for the observed changes in surface q. There is only weak evidence for the presence of natural forcing influences using the simple comparisons employed herein.

5.5 TABLES AND FIGURES FOR CHAPTER 5

REGION	Land and Marine *q* Timeseries Correlation		*q* Trends (g kg^{-1} 10yr^{-1})	
	r (1973-2003)	r (1982-2003)	Land	Marine
Global	0.71	0.76	0.11**	0.07**
Northern Hemisphere	0.69	0.70	0.12**	0.08**
Tropics	0.79	0.77	0.16**	0.10**
Southern Hemisphere	0.22	0.23	0.01	0.01

Table 5.1: Statistical values for a comparison of the land and marine gridded datasets. The Global region covers 70 ^{o}S to 70 ^{o}N. The Northern Hemisphere region covers 20 ^{o}N to 70 ^{o}N. The Tropical region covers from 20 ^{o}S to 20 ^{o}N. The Southern Hemisphere covers from 70 ^{o}S to 20 ^{o}S. The *r* values are linear Pearson correlation coefficients. Shaded boxes highlight strongest *r* values and strongest trends for each region. Trends are calculated using the REML method (Box 3.4). Significance at 5 % is shown with a * and at the 1 % with **.

Region	Trend	Seasonally Averaged Trend			
		DJF	MAM	JJA	SON
HadCRUH *q* (g kg^{-1} 10yr^{-1})					
Global	0.07**	0.06*	0.06**	0.08**	0.07**
Northern Hemisphere	0.08**	0.06**	0.06**	0.15**	0.10**
Tropics	0.10**	0.10*	0.11**	0.10**	0.11**
Southern Hemisphere	0.02	-0.00	0.01	*-0.03*	0.00
HadCRUH *RH* (% 10yr^{-1})					
Global	-0.06	-0.10	-0.10	-0.08	*-0.11*
Northern Hemisphere	0.00	-0.03	*-0.15**	0.18**	0.13**
Tropics	*-0.10***	-0.11	-0.10	-0.13	*-0.15*
Southern Hemisphere	*-0.10*	-0.22	-0.04	*-0.31**	-0.26
HadCRUT3 (^{o}C 10yr^{-1})					
Global	0.18**	0.20**	0.18**	0.18**	0.17**
Northern Hemisphere	0.24**	0.31**	0.23**	0.25**	0.22**
Tropics	0.17**	0.19**	0.18**	0.18**	0.18**
Southern Hemisphere	0.10**	0.10**	0.13**	0.10**	0.08**

Table 5.2: Trends for surface *q*, *RH* and *T*. Shaded boxes (*italics*) highlight the region /season of maximum positive (negative) trend. Regions are as described in Table 5.1. Seasonal trends are created using the LSR technique (Box 3.4). All other trends are calculated using the REML method (Box 3.4). Significance at 5 % is shown with a * and at the 1 % with **.

Category	Description	Regions
Actual and Relative Moistening	$q \geq 0.05$ g kg^{-1} 10yr^{-1} and $RH \geq 0.05$ % 10yr^{-1}	CAS, CNA, ENA*, IND, NAS*, SAS, SEA*, SSA and TIB*
Actual and Relative Drying	$q \leq -0.05$ g kg^{-1} 10yr^{-1} and $RH \leq -0.05$ % 10yr^{-1}	None
Actual Moistening and Relative Drying	$q \geq 0.05$ g kg^{-1} 10yr^{-1} and $RH \leq -0.05$ % 10yr^{-1}	AMZ*, CGI, MED*, NPA, SAF, SAH, SAT and SEU*
Small Actual Change and Relative Drying	$q < 0.05$ g kg^{-1} 10yr^{-1} and $RH \leq -0.05$ % 10yr^{-1}	CAM, EAF, NAU, SAU, SPA*, and WNA
Small Actual Change and Relative Moistening	$q < 0.05$ g kg^{-1} 10yr^{-1} and $RH \geq 0.05$ % 10yr^{-1}	ALA
Actual Moistening and Small Relative Change	$q \geq 0.05$ g kg^{-1} 10yr^{-1} and $RH > -0.05$ and < 0.05 % 10yr^{-1}	CAR, EAS, NAT, NEU and WAF
Small Actual and Relative Trend	$q < 0.05$ g kg^{-1} 10yr^{-1} and $RH < 0.05$ % 10yr^{-1} and $RH > -0.05$ % 10yr^{-1}	None

Table 5.3: Categorising the twenty nine regions by trends in *q* and *RH*. Trends are calculated using the LSR method (Box 3.4). Region abbreviations and locations are shown in Figure 5.2. Starred regions are where both *q* and *RH* trends are significant at the 1 % or 5 % level. The accompanying timeseries and trends are shown as Figures 5.3a and b (split over two pages).

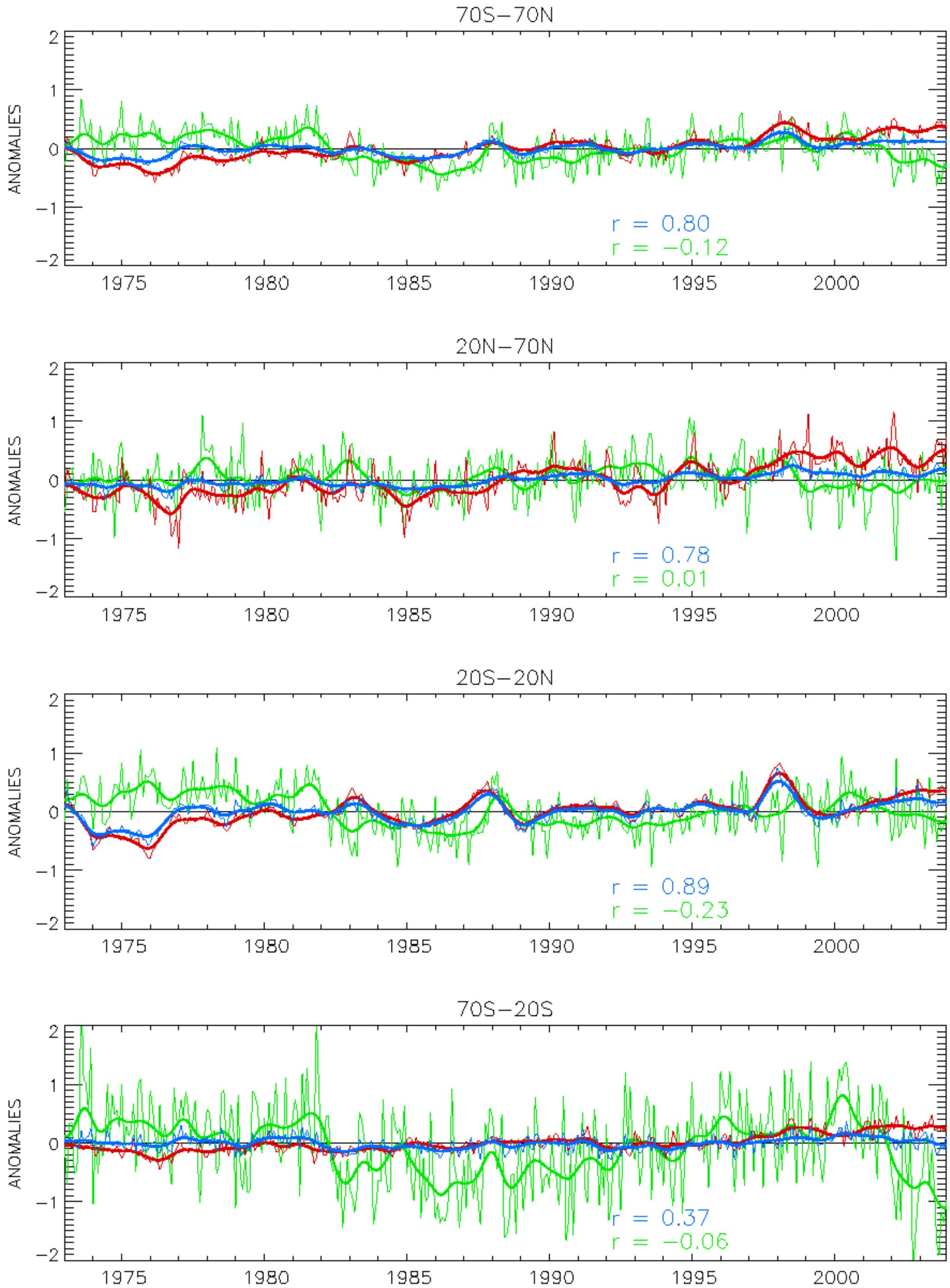

Figure 5.1: Regionally averaged monthly mean anomaly timeseries for *q*, *RH* and *T* with smoothing. *RH* (green) and *q* (blue) timeseries are from HadCRUH and *T* (red) timeseries are from HadCRUT3. The *T* data have been re-normalised to the 1974 to 2003 climatology period. The data have been smoothed using a 21 point Gaussian weighted filter for the low frequency component of the timeseries. *T*-*q* and *T*-*RH* correlations are shown in blue and green respectively. Units are in % for *RH*, ^{o}C for *T* and g kg^{-1} for *q*.

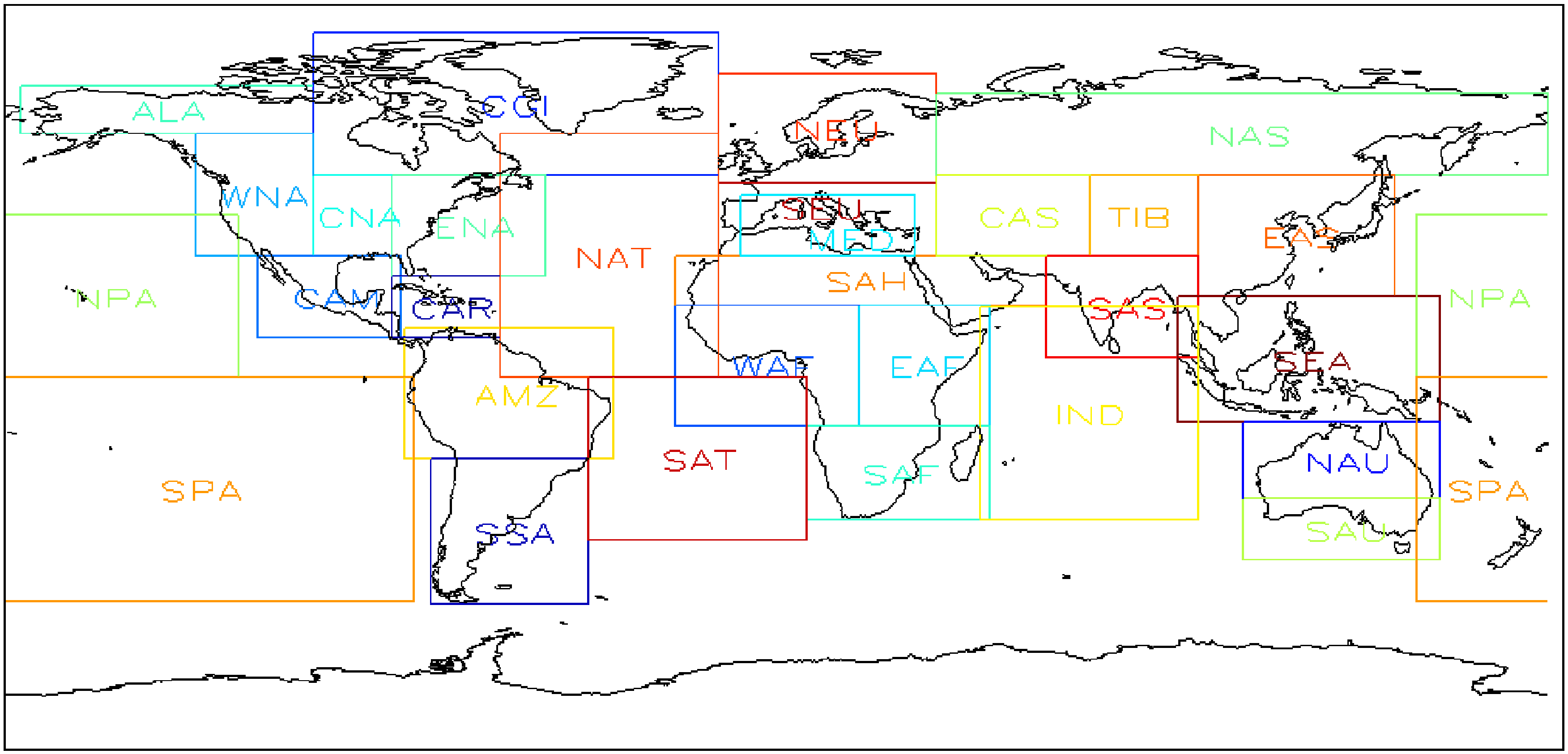

Figure 5.2: Map of the twenty nine regions and abbreviations. ALA = Alaska and North West Canada. AMZ = Amazonia. CAM = Central America. CAR = Caribbean. CAS = Central Asia. CGI = East Canada, Greenland and Iceland. CNA = central North America. EAF = East Africa. EAS = East Asia. ENA = eastern North America. IND = Indian Ocean. MED = Mediterranean. NAS = North Asia. NAT = North Atlantic. NAU = North Australia. NEU = North Europe. NPA = North Pacific. SAF = South Africa. SAH = Sahara. SAS = South Asia. SAT = South Atlantic. SAU = South Australia. SEA = South East Asia. SEU = South Europe and North Africa. SPA = South Pacific. SSA = southern South America. TIB = Tibetan Plateau. WAF = West Africa. WNA = western North

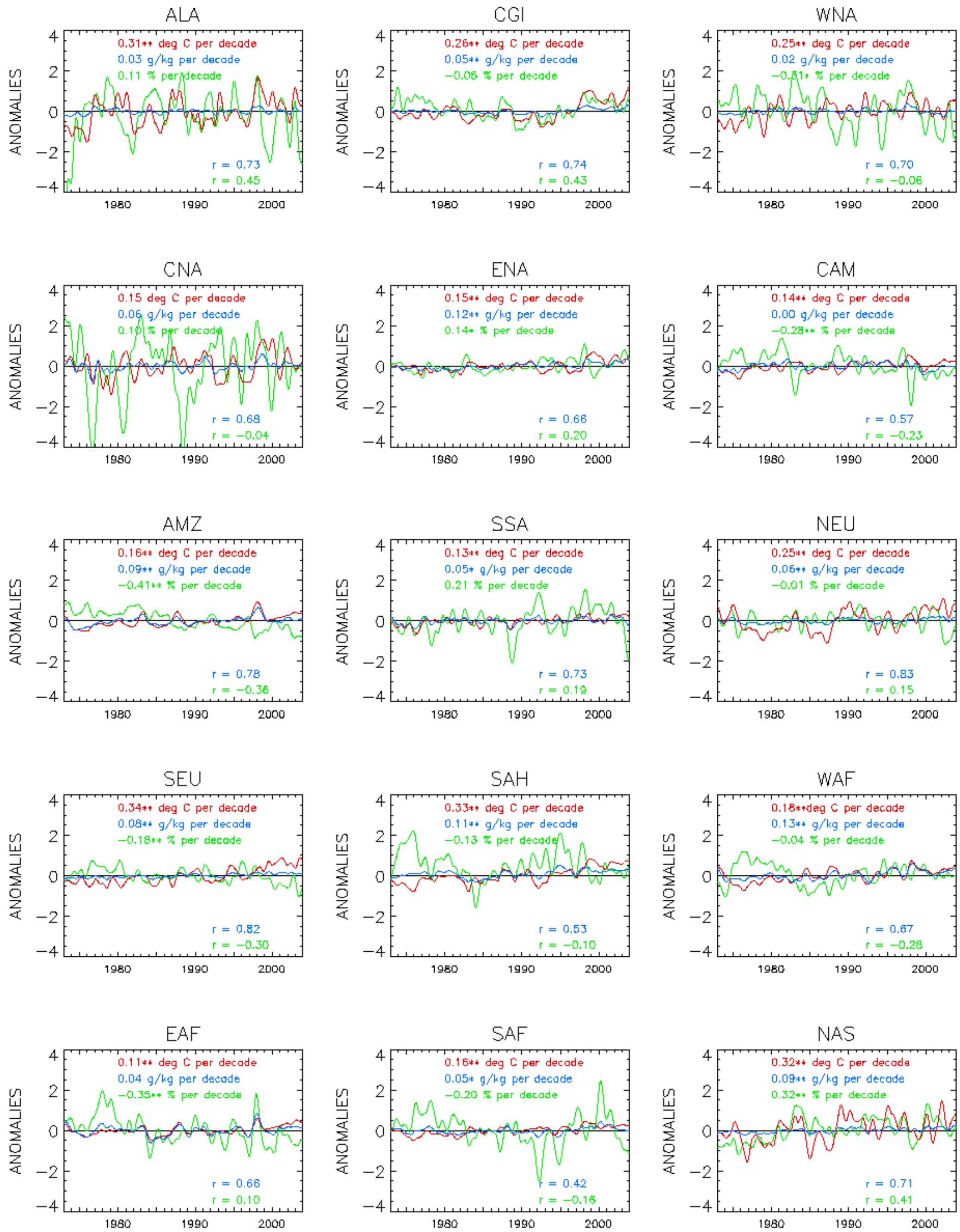

Figure 5.3a: Regional analyses of monthly mean anomaly timeseries (smoothed) and trends in *q*, *RH* and *T*. Continued on next page. *RH* (green) and *q* (blue) timeseries are from HadCRUH and *T* (red) timeseries are from HadCRUT3. The *T* data have been re-zeroed to the 1974 to 2003 climatology period. The data have been smoothed using a 21 point Gaussian weighted filter for the low frequency component of the timeseries. Trends are calculated using the LSR method (Box 3.4). Significance at 5 % is indicated by * and at 1 % by **. Region abbreviation descriptions can be found in Figure 5.2. *T*-*q* and *T*-*RH* linear Pearson correlation coefficients (*r*) are shown in blue and green respectively. Units are in % for *RH*, °C for *T* and g kg^{-1} for *q*.

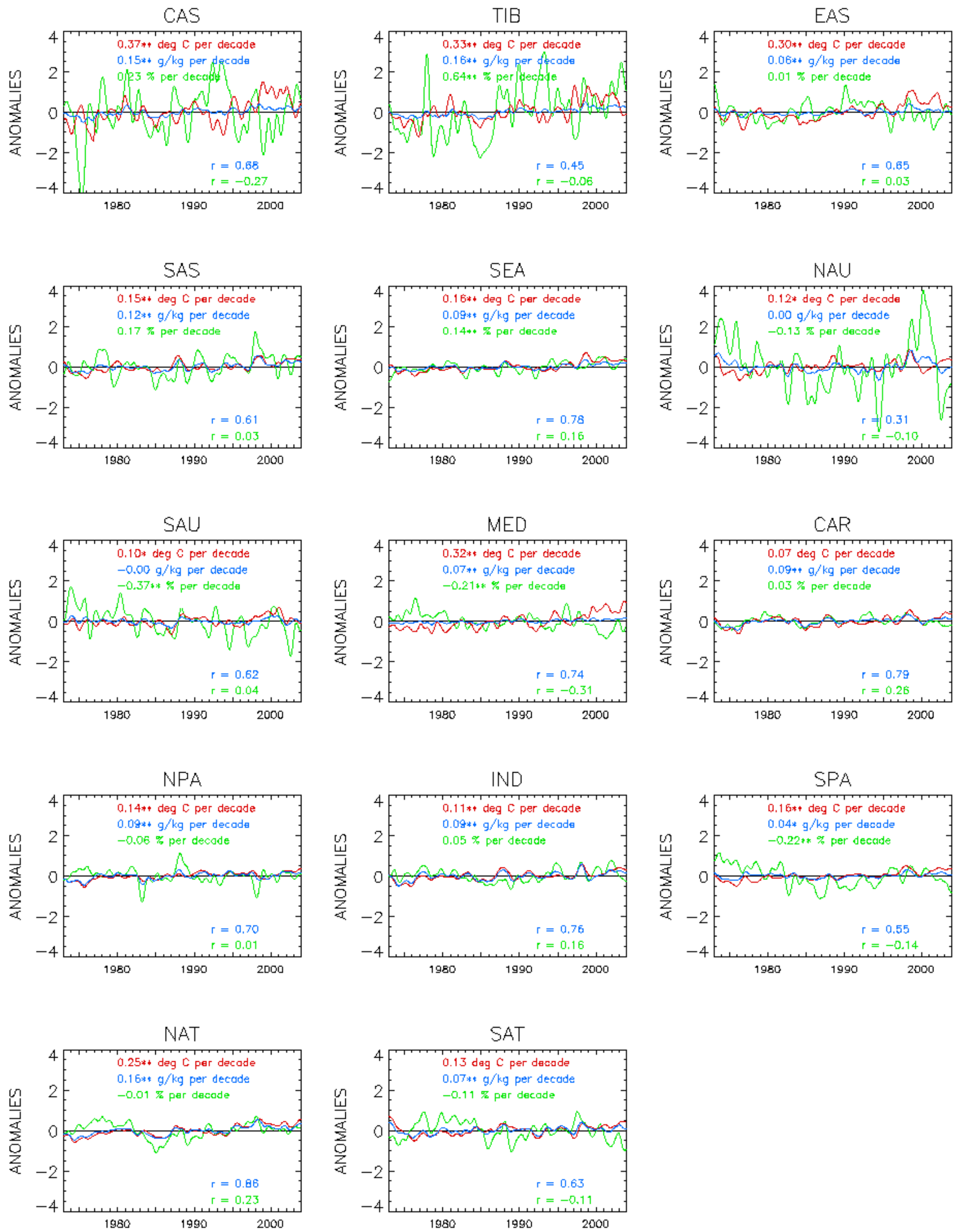

Figure 5.3b: Regional analyses of monthly mean anomaly timeseries (smoothed) and trends in *q*, *RH* and *T*. Continued from previous page. *RH* (green) and *q* (blue) timeseries are from HadCRUH and *T* (red) timeseries are from HadCRUT3. The *T* data have been re-zeroed to the 1974 to 2003 climatology period. The data have been smoothed using a 21 point Gaussian weighted filter for the low frequency component of the timeseries. Trends are calculated using the LSR method (Box 3.4). Significance at 5 % is indicated by * and at 1 % by **. Region abbreviation descriptions can be found in Figure 5.2. *T*-*q* and *T*-*RH* linear Pearson correlation coefficients (*r*) are shown in blue and green respectively. Units are in % for *RH*, ^{o}C for *T* and g kg^{-1} for *q*.

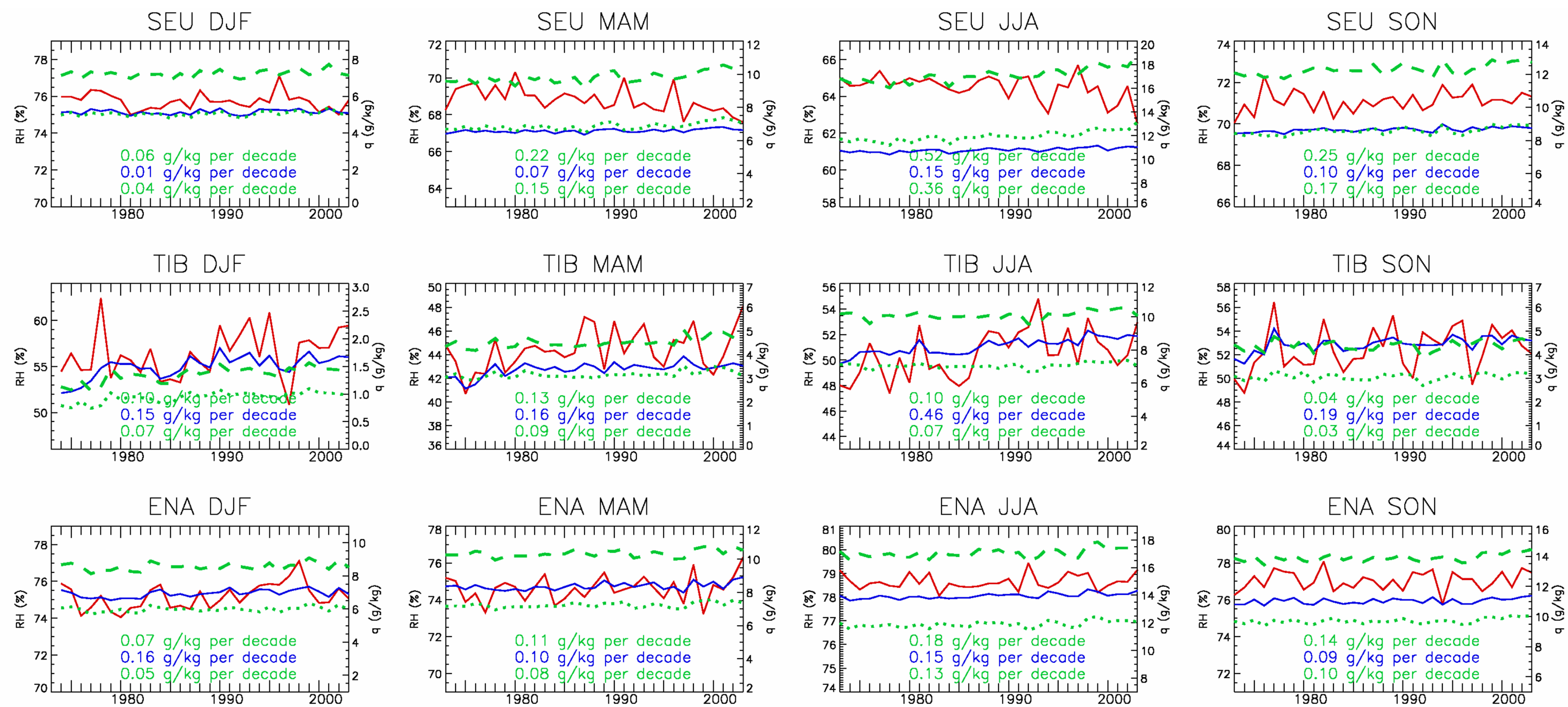

Figure 5.4a: Estimated and observed absolute *q* trends based on observed absolute *T* from five regions. Continued on next page. Estimated *q* is calculated based on observed absolute *T* from HadCRUT3 and a constant *RH* of 70 % (dotted green) and 100 % (dashed green). Observed *q* is in blue and observed *RH* in red. MPS trends (Box 3.4) are calculated for estimated *q* at 100 % *RH* (top), estimated *q* at 70 % *RH* (bottom) and observed *q* (middle). The South Europe and North African region (SEU) is chosen as an example of a region of significantly increasing *q* and significantly decreasing *RH*. The Tibetan Plateau (TIB) and easter North American (ENA) regions are chosen as landlocked and coastal regions respectively of significantly increasing *q* and *RH*. The Indian Ocean (IND) and East Canada, Greenland and Iceland (CGI) regions are chosen as marine and land based regions respectively of significantly increasing *q* and constant *RH*. Region abbreviation descriptions can be found in Figure 5.2.

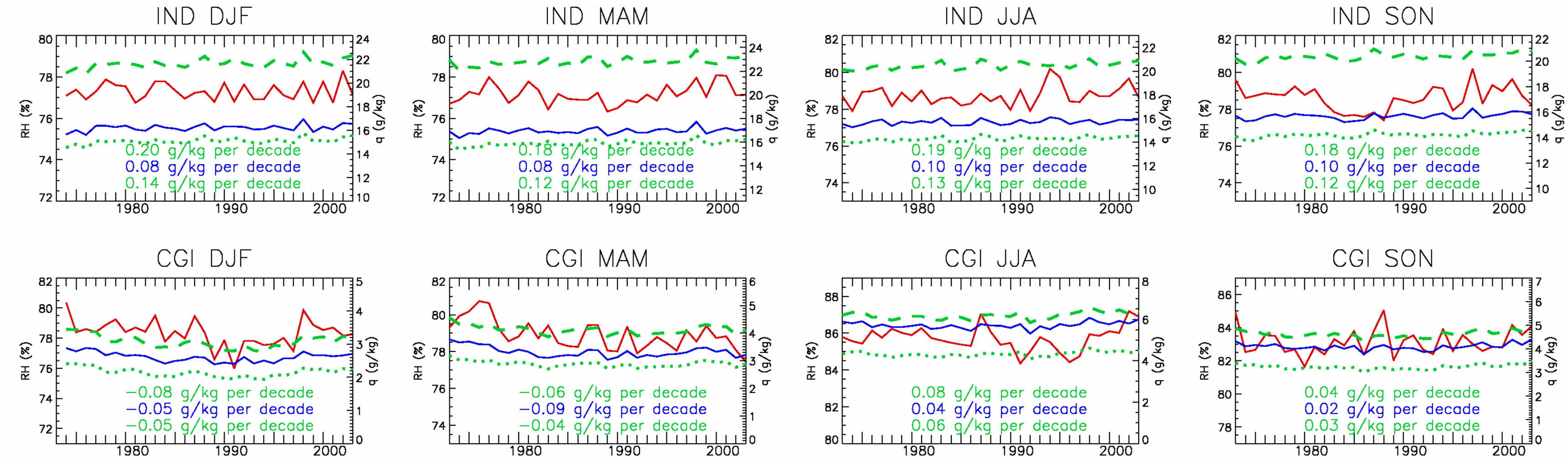

Figure 5.4b: Estimated and observed absolute *q* trends based on observed absolute *T* from five regions. Continued from previous page. Estimated *q* is calculated based on observed absolute *T* from HadCRUT3 and a constant *RH* of 70 % (dotted green) and 100 % (dashed green). Observed *q* is in blue and observed *RH* in red. MPS trends (Box 3.4) are calculated for estimated *q* at 100 % *RH* (top), estimated *q* at 70 % *RH* (bottom) and observed *q* (middle). The South Europe and North African region (SEU) is chosen as an example of a region of significantly increasing *q* and significantly decreasing *RH*. The Tibetan Plateau (TIB) and easter North American (ENA) regions are chosen as landlocked and coastal regions respectively of significantly increasing *q* and *RH*. The Indian Ocean (IND) and East Canada, Greenland and Iceland (CGI) regions are chosen as marine and land based regions respectively of significantly increasing *q* and constant *RH*. Region abbreviation descriptions can be found in Figure 5.2.

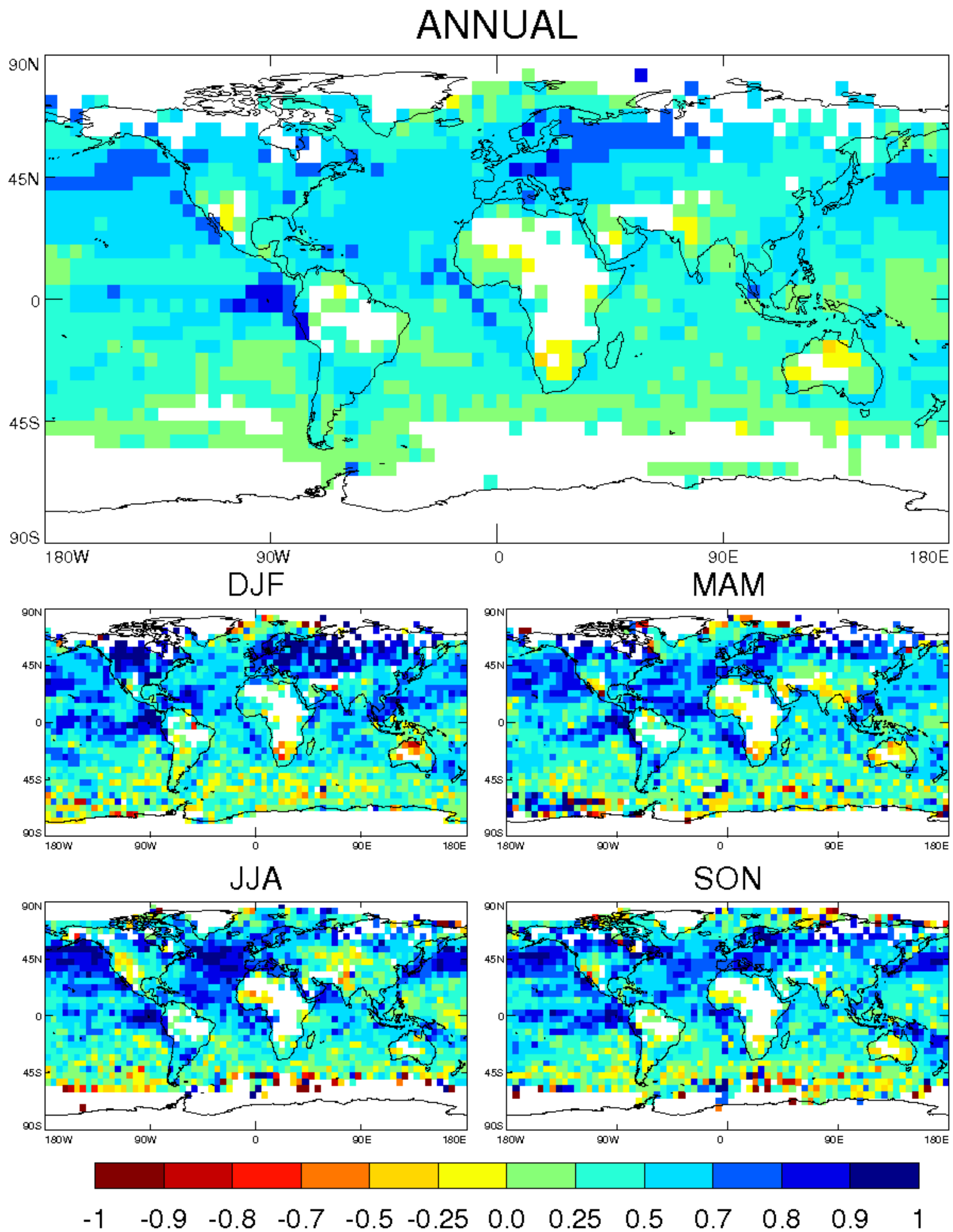

Figure 5.5: Linear Pearson correlations coefficients of monthly mean anomaly *T* and *q* and seasonal anomaly *T* and *q* at the grid-box scale. Observed *T* values are from HadCRUT3, normalised to the 1974 to 2003 climatology and matched spatially and temporally to the HadCRUH *q* dataset coverage.

Figure 5.6: January and July climatologies in *q* for HadCM3 CONTROL and HadCRUH minus HadCM3 CONTROL. For the CONTROL a mean climatology is taken from the climatologies for all 27 segments of the CONTROL run where the climatology period is from year 2 to 27 (out of a 31 year period) to correspond with the climatology period 1974 to 1999 in the observations. This period is used for comparison with model output. Units are in g kg^{-1}.

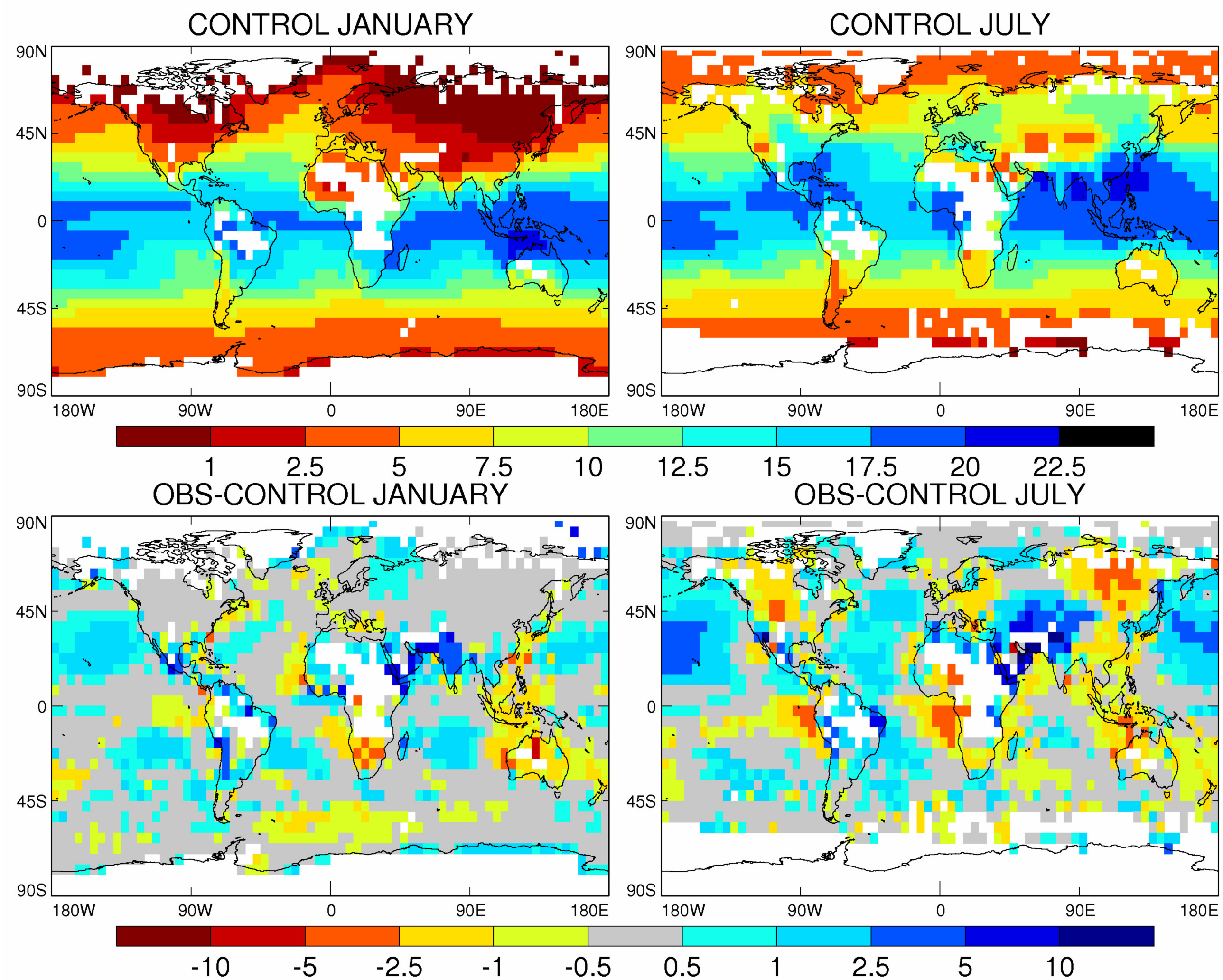

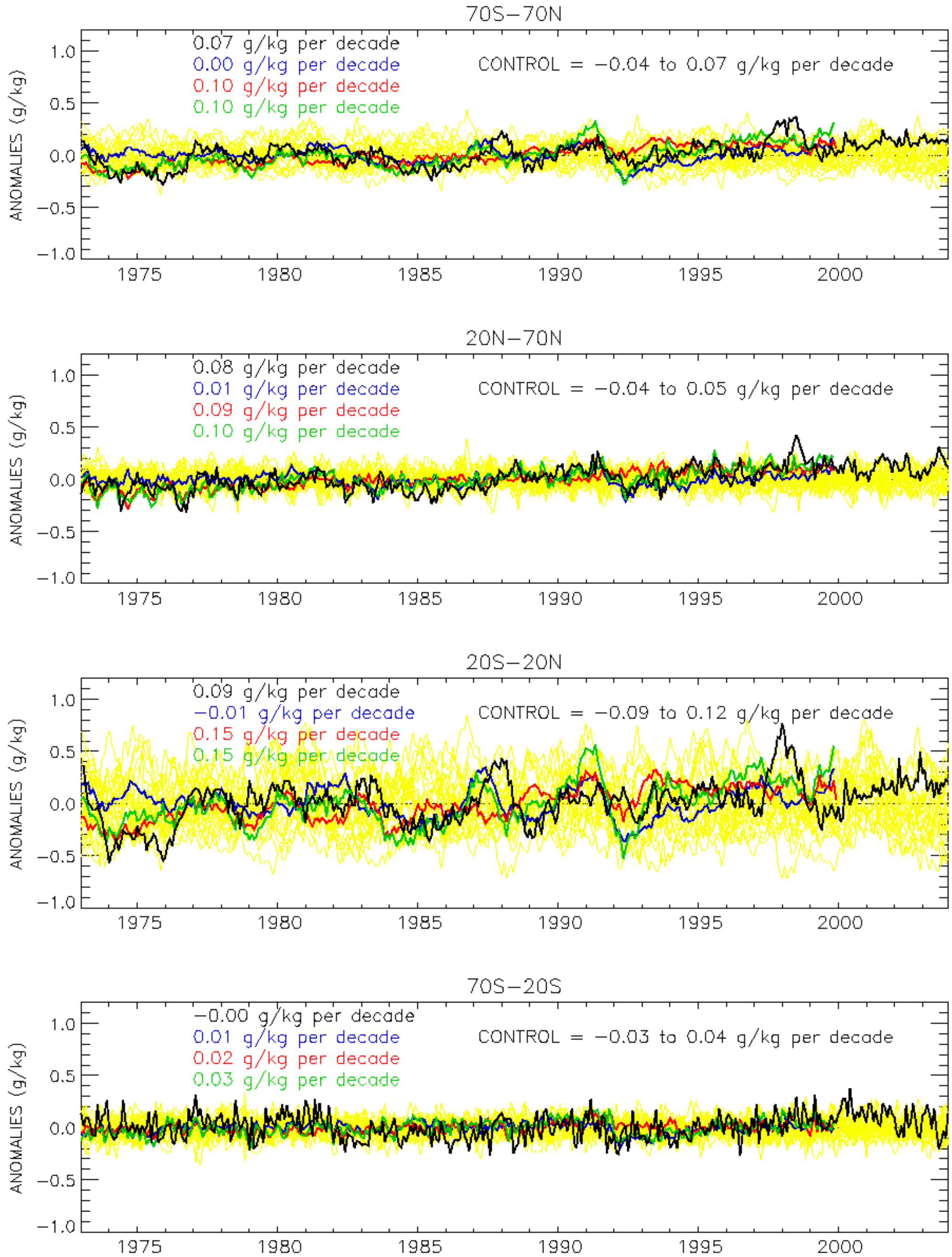

Figure 5.7: Regionally averaged monthly mean anomaly timeseries and trends for observed and ensemble model runs in *q*. HadCRUH *q* (black) is re-zeroed to a 1974 to 1999 climatology period in keeping with ensemble model runs. Twenty-seven HadCM3 control runs (yellow) are used to provide a measure of natural variability with which to gauge significance of trends in *q*. ANTHRO, NATURAL and ANT+NAT ensemble timeseries are shown in red, blue and green respectively. MPS trends (Box 3.4) are calculated over the period 1973 to 1999 and shown in respective colours. Maximum and minimum (95th and 5th percentiles) trends are shown for CONTROL runs in black.

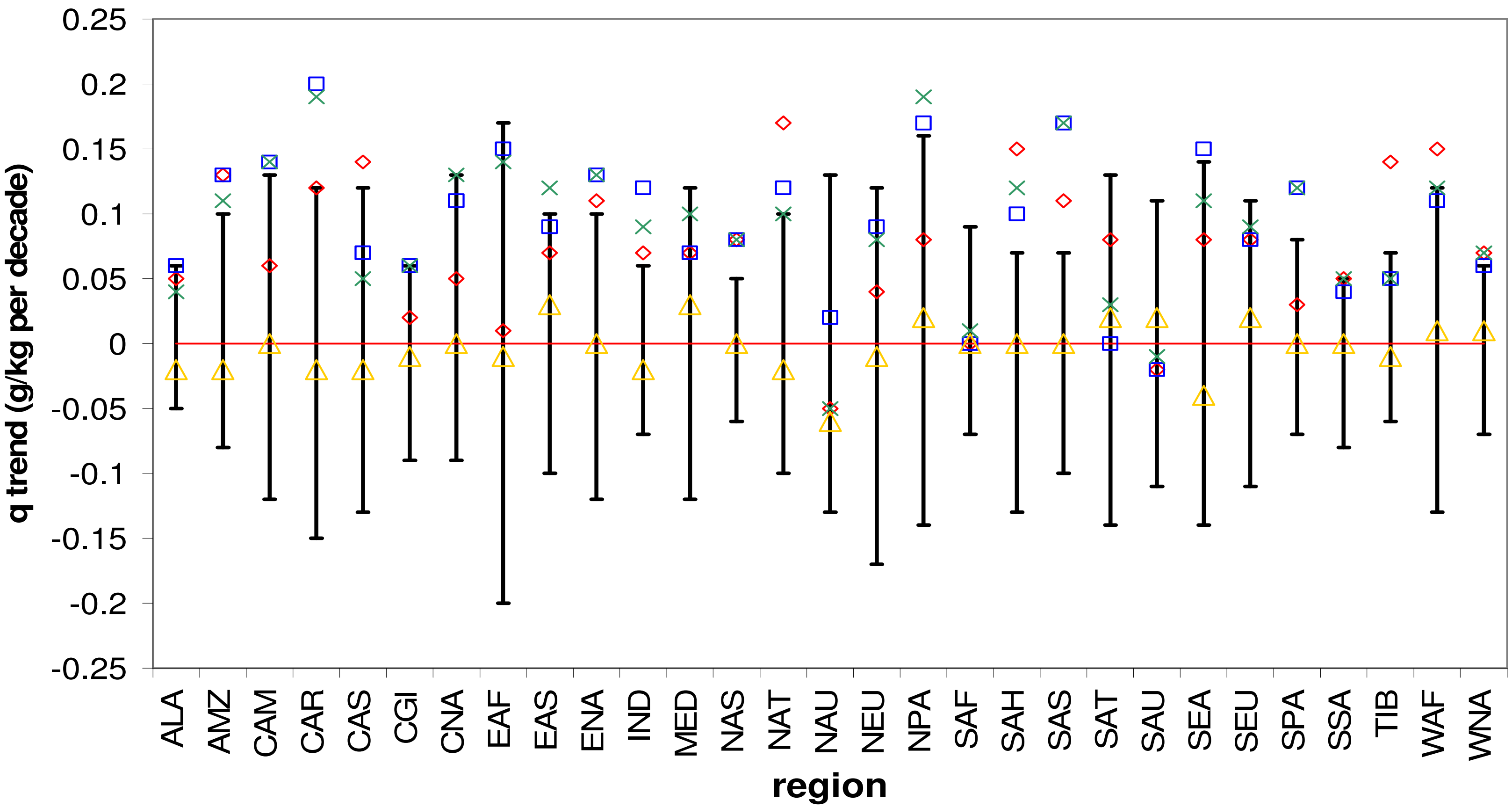

Figure 5.8: Comparison of observed and model *q* trends for twenty nine regions. MPS trends (Box 3.4) are calculated over the period 1973 to 1999 for the observations (red diamonds), ANTHRO ensemble (blue squares), NATURAL ensemble (orange triangles) and ANT+NAT ensemble (green crosses). The range of trends (95th and 5th percentiles) from the CONTROL segments is also shown as a measure of natural variability. For a summary of findings refer to Fig. 5.9. Region abbreviation descriptions can be found in Figure 5.2.

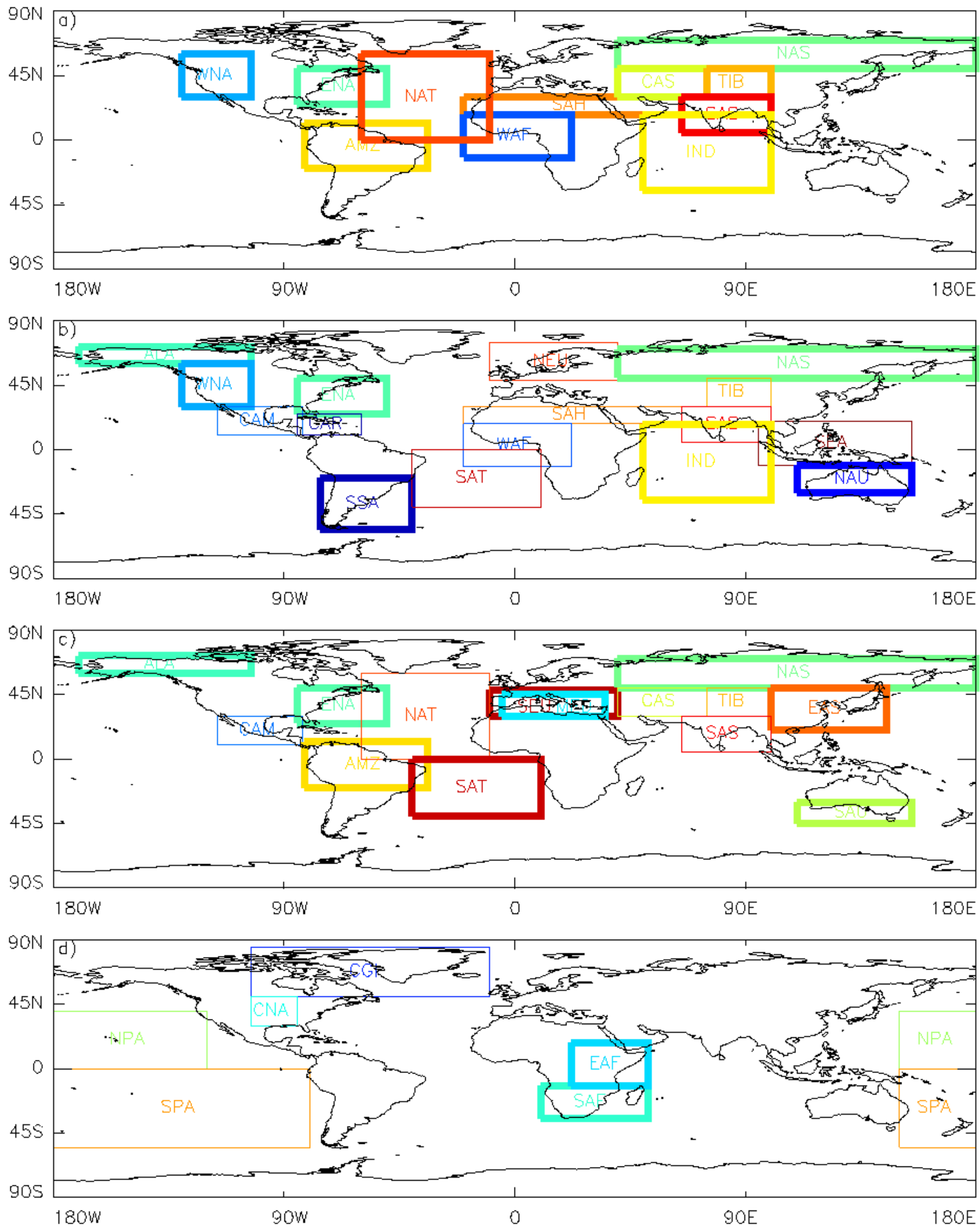

Figure 5.9: Comparison of observed and model *q* trends for the twenty nine regions. Plot a) shows regions where the observed trends are greater than that expected due to natural internal variability as prescribed by the 5th to 95th percentile range of the 27 CONTROL segment trends. Plot b) shows regions where the ANT+NAT trends are closest to the observed trends. Plot c) shows regions where the ANTHRO trends are closest to the observed trends. Plot d) shows regions where the NATURAL trends are closest to the observed trends. For plots b to d thick lines show regions where observed and modelled trends are within 0.02 g kg^{-1}. For actual values see Fig. 5.8 and for region acronym definitions see Fig. 5.2.

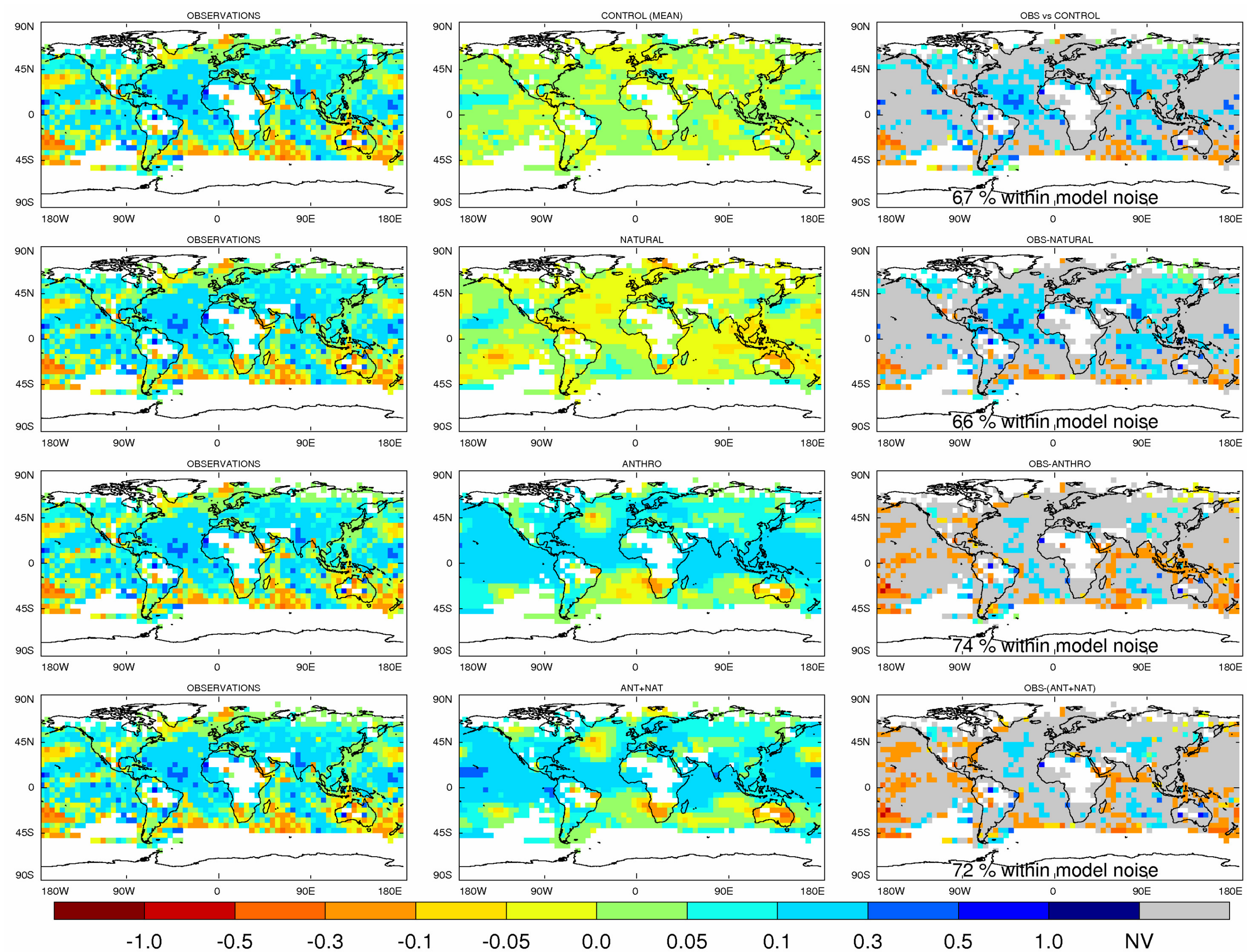

Figure 5.10: Comparison of observed and modelled *q* trends at the grid-box scale. MPS trends (Box 3.4) are calculated for the period 1973 to 1999 and units are in g kg $^{-1}$ 10yr $^{-1}$. In the case of OBS vs CONTROL the greyed out grid-boxes represent regions where observed trends are within the range of natural variability for that grid-box. Non-greyed trends represent regions of significant climate change signal such that it cannot be expected to occur due to natural variability. For all other plots greyed out areas are where the difference between observed and modelled trends is within the measure of natural variability for that grid-box. Natural variability is estimated from the 5th and 95th percentile trends from 27 CONTROL segments.